AIAA Guidance, Navigation, and Control Conference and Exhibit
21 - 24 August 2006, Keystone, Colorado

AIAA 2006-6227

Eulerian Trilogy

Dengfeng Sun*, Samuel D. Yang*, Issam Strub*, Alexandre M. Bayen †
University of California, Berkeley, CA 94720-1710, USA.

Banavar Sridhar‡, Kapil Sheth‡
NASA Ames Research Center, Moffett Field, CA 94035, USA.

Three Eulerian models are implemented on a network graph model of air traffic flow. The underlying network is constructed using one year of ASDI/ETMS data. The three models are applied to high altitude traffic for a full Air Route Traffic Control Center of the National Airspace System and surrounding airspace. Simulations are carried out for a full day of data, to assess the predictive capabilities of the respective models. The models' predictions are compared to the recorded flight data (ASDI/ETMS). Several error metrics are used to characterize the relative accuracy of the models. The efficiency of the respective models is compared in terms of computational time and memory requirements for the scenarios of interest. A discussion of the three models' structural differences explains why one model may outperform another.

I. Introduction

The almost uninterrupted growth of US air traffic over the last few decades has motivated the design of a semi-automated *Air Traffic Control* (ATC) system to help Air Traffic Controllers manage the increasing complexity of traffic flow in the en route airspace.[1] ATC is operated at the sector level, where a sector is a small portion of the airspace controlled by a single human Air Traffic Controller. *Traffic Flow Management* (TFM) typically deals with traffic at the *Center* level, i.e. 10 to 20 sectors. TFM problems include maintaining the aircraft count in each sector below a legal threshold in order to ease the human ATC workload, as well as to ensure the safety of the flights.[2] This task is quite cumbersome; furthermore, extensive traffic forecast simulations (including all airborne aircraft) are computationally too expensive to include systematic investigations of traffic patterns that lead to sector overload. As a result, a new class of traffic flow models has emerged from recent studies: *Eulerian* models, which are control volume based. This is in contrast to *Lagrangian* models, which are trajectory-based and take into account all aircraft trajectories.[3] Unlike Lagrangian models which focus on the history of a given agent therefore using the position vector of the agent and time as variables, the Eulerian models provides a picture of the spatial distribution of the flow in function of position in space and time.

Eulerian models have two main advantages over Lagrangian models. (*i*) They are computationally tractable, and their computational complexity does not depend on the number of aircraft, but only on the size of the physical problem of interest. (*ii*) Their control theoretic structure enables the use of standard methodologies to analyze them, such as control theory or optimization.

This article presents the comparison between three Eulerian models of the *National Airspace System* (NAS), to assess their respective accuracy, computational efficiency, and predictive capabilities. This study is thus motivated by the need to efficiently model the NAS. For fairness of the comparison, we are implementing the three models on the same network developed in earlier work, based on one year of ASDI/ETMS data.

The field of Eulerian network modeling for the NAS has been pioneered by the award winning AIAA article of Menon et al.[4]. This article is strongly inspired by hydrodynamic theory for highway traffic flow, in particular the work of Lighthill, Whitham and Richards,[5,6] and its discrete counterparts in the highway

*Ph.D. Students, Department of Civil and Environmental Engineering.
†Assistant Professor, Department of Civil and Environmental Engineering.
‡NASA Ames Research Center, Moffett Field, CA 94035, USA.

traffic literature.[7,8] This framework is sometimes referred to as the *LWR theory*.[9] To the best of our knowledge, Menon et al.[4] were the first to model air traffic flow using an Eulerian framework, i.e. focusing on control volumes rather than single aircraft trajectories.[10–13] This work was subsequently extended by the same authors. It triggered a large interest in the *Air Traffic Management* (ATM) community, leading to several articles inspired by their original approach.[12,14] This model was later adapted to include a stochastic framework,[15,16] in which data aggregation procedures enable predictions of flows in the expected sense. For the present study, the Menon model[12] is modified to fit a graph structure developed in our earlier work.[17] Adjoint based techniques[18] were subsequently developed for a fully continuous[19] NAS model (i.e. using partial differential equations), which was also used for modeling behavior of single agents (airlines) in the NAS.[20,21] In order to alleviate the problems due to network splits (this problem will be explained in detail later in this article and affects all previous models), a delay system model based on network flow techniques[22] was finally proposed[17] and successfully implemented, which does not suffer such shortcomings.

In this article, we present a modified version of the Menon model, adapted to fit a general network topology. We summarize a delay-based model presented in our earlier work.[17] Finally, we present a new application of the Lax Wendroff scheme to a PDE model developed earlier.[19] We implement and compare the three models above on the same benchmark problem. We will thus compare the modified Menon model, the more recent delay system model,[17] and the fully continuous PDE model.[19]

This paper is organized as follows. In the next section, the formulation of the three models are summarized. Section III assesses the predictive capability of each model through a careful validation against recorded ASDI/ETMS data. Section IV compares the predictive capabilities of the different models, computational time and memory requirements. A discussion follows that highlights the structural differences between the three models and explains why one model may outperform another. Finally conclusions are presented in Section V.

II. Models

A. The Modified Menon Model[12] (MMM)

This section is based on earlier work by Menon et al.[12]. The model has been modified to fit the structure of the graph model that will be discussed in Section II D. First, the Menon model is summarized followed by the details of the modifications.

The Menon model is an Eulerian traffic flow model in which the air traffic flow is spatially aggregated into control volumes.[12] It is based on the *LWR theory* in which the traffic flowing into a control volume changes the density of aircraft in the control volume and, hence, changes the outflow from the control volume. In the present work, the Menon model has been adapted by keeping track of the flow rates into and out of the control volumes as well as the aircraft count within each volume. We will thus refer to the improved version of the model as the *Modified Menon Model* (MMM). The model is also able to account for ATC actions as well as handle merging and diverging air traffic flow. The model consists of two parts, the one-dimensional control volume model and the merge and diverge routing structure.

The one-dimensional control volume model takes air traffic flow as a network of inter-connected control cells where the air traffic flows through a series of control volumes. One way to think of the model is as a sequence of cells, where each cell is a control volume. The air traffic flow and aircraft counts in a network, can be described by the discrete-time difference equation,

$$x_j(i+1) = x_j(i) + \tau_j[y_{j-1}(i) - y_j(i)] \tag{1}$$

In the above equation, $x_j(i+1)$ is the aircraft count of control volume j at time $i+1$. The flow into j is $y_{j-1}(i)$ and $y_j(i)$ is the flow out of j. The time step τ_j is computed by dividing the cell dimension, Ω_j, by the aircraft speed in the cell, v_j ($\tau_j = \Omega_j/v_j$). In other words, τ_j is the time an aircraft takes to travel through the cell.

The effects of delaying aircraft due to ATC is accounted for by recirculating some of the air traffic flow in a control volume. The recirculated air traffic flow in control volume j is defined as u_j. The physical constraint on u_j is that at time i it can not be greater than the existing flow in the cell and it can not be less than 0,

$$0 \leq \tau_j u_j(i) \leq x_j(i) \tag{2}$$

Including u_j and writing down the equation for y_j, the model can be written as a linear, discrete-time dynamic system,

$$x_j(i+1) = a_j x_j(i) + \tau_j u_j(i) + \tau_j y_{j-1}(i) \tag{3}$$

$$y_j(i) = b_j x_j(i) - u_j(i) \tag{4}$$

The coefficients, a_j, b_j, and τ_j handle the conversion between the air traffic flow, y_j, and the aircraft count, x_j. In other words, at a given time step, a_j is the portion of aircraft remaining in the volume, and b_j is the portion of air traffic flow leaving the volume. As was noted earlier, τ_j is the length of time needed for the aircraft to travel the length of the control volume. The coefficients are defined in terms of Ω_j, the control volume length, and v_j, the aircraft speed.

$$a_j = (1 - v_j \tau_j / \Omega_j), \quad b_j = v_j / \Omega_j, \quad \tau_j = \Omega_j / v_j \tag{5}$$

The original Menon model assumes that velocity is constant within a given control volume. This means that a_j is always zero (see equation (13) in the original article[12]). That is, if there is no control from u_j, then all the aircraft in the volume travel to the subsequent volume on the next time step.

Intuitively, what is happening in equations (3) and (4) is that the aircraft count in a given control volume at time $i+1$ depends on the number of aircraft in the volume at time i, the number of aircraft that flow into the volume, the number of aircraft that are recirculated and the number of aircraft that flow out of the volume. Over multiple time steps, aircraft will move through successive cells.

In a network of inter-connected control volumes, there may be points where air traffic coming from different directions merge into a single flow. This type of situation is referred to as a merge node. Furthermore, there may be points where the air traffic in one direction diverges into multiple flows. This type of situation is referred to as a diverge node. Because the nodes do not retain any aircraft, the conservation principle implies that for merge nodes, the resulting air traffic flow is the sum of all air traffic flows into that node. For example, if the air traffic flows q_{k-1} and q_{k-2} merge into q_k,

$$q_k = q_{k-1} + q_{k-2} \tag{6}$$

Likewise, diverge nodes can make use of the same conservation principle and the flow along a path from a diverge node is a proportion of the flow coming into the diverge node. The proportion is defined as the divergence parameter, β, and is the ratio of aircraft travelling out of the diverge node along a given path over the aircraft travelling into the diverge node. In the following example, the air traffic flow diverges from the q_k to q_{k+1} and q_{k+2},

$$q_{k+1} = \beta q_k, \quad q_{k+2} = (1 - \beta) q_k \tag{7}$$

As mentioned earlier, since the MMM is implemented on a graph model of traffic flow constructed in the articles[17,23] and discussed in Section II D, a number of modifications were made to improve the original Menon model described in the article.[12]

1. The flights in the MMM are aggregated according to the links of the graph structure defined in our earlier work, and not the graph model presented in their original article.[12] This will ensure fairness of the comparison with the other models.

2. A link length (physical distance) is determined from flights in the data. That is, flights in the data are aggregated according to the links in the graph. A link's entry and exit locations are determined by those flights' link entries and exits. The entry and exit locations are used in computing the link's length.

3. The MMM contains merge-diverge nodes. A merge-diverge node is one that has both merging and diverging flows at the same time. The original Menon model does not have such nodes.

4. A merge-diverge node can have n ($n \geq 2$) outflows, whose β values are determined from the data, whereas in the original Menon model n is limited to two.

B. The delay system model

The delay system model is a new Eulerian traffic flow model developed by Robelin et al.[24]. It is a graph-theoretic model of traffic flow. Air traffic flow on this graph is modeled as a discrete time dynamical system. Under the assumption that air traffic flow can be accurately represented by an aggregated travel time, the behavior of aircraft flows on a single link can be modeled by a deterministic linear dynamical system with unit time delay, defined as follows.[24]

$$x_i(k+1) = A_i x_i(k) + B_i^f f_i(k) + B_i^u u_i(k) \tag{8}$$

$$y(k) = C_i x_i(k) \tag{9}$$

where $x_i(k) = [x_i^{m_i}(k), ..., x_i^1(k)]^T$ is the state vector, whose elements represent the corresponding aircraft counts in each cell of link i at time step k, and m_i is the number of cells in the link. The [forcing] input, $f_i(k)$, is a scalar which denotes the entry count onto link i during a unit time interval from k to $k+1$, and the [control] input, $u_i(k)$ is an $m_i \times 1$ vector, representing holding pattern control. The output, $y(k)$, is the aircraft count in a user-specified set of cells at time step k. The nonzero elements of the $m_i \times 1$ vector C_i correspond to the cells in the user-specified set, and are equal to one. A_i is an $m_i \times m_i$ nilpotent matrix with 1's on its super-diagonal. $B_i^f = [0, ..., 0, 1]^T$ is the forcing vector with m_i elements, and B_i^u is the $m_i \times m_i$ holding pattern matrix, in which all nonzero elements are 1 on the diagonal and -1 on the super-diagonal. Please see article[23] for more details about the model.

Because there is no interconnection between different links in one sector, it is straightforward to extend this modeling technique to set up a sector level model as follows. Suppose there are n links in a sector, then the state space equations for the model at the sector level can be described as:

$$x(k+1) = Ax(k) + B^f f(k) + B^u u(k) \tag{10}$$

$$y(k) = Cx(k) \tag{11}$$

where $x(k) = [x_n(k), ..., x_1(k)]^T$ denotes the state, and $f(k) = [f_n(k), ..., f_1(k)]^T$ is the [forcing] input vector (the entry count onto the sector). The [control] input vector $u(k) = [u_n(k), ..., u_1(k)]^T$. $y(k)$ represents the aircraft count in a user-specified set of cells at time step k. The matrices A, B^f, and B^u are block diagonal, such that $A = \text{diag}(A_n, \ldots, A_1)$, $B^f = \text{diag}(B_n^f, \ldots, B_1^f)$, and $B^u = \text{diag}(B_n^u, \ldots, B_1^u)$. The vector C is given by $[C_n, ..., C_1]$. The quantities, $x_i(k)$, $f_i(k)$, $u_i(k)$, A_i, B_i^f, B_i^u and C_i are all defined by Equations (8) – (9).

When a center level model is created, it is necessary to include *merge/diverge* nodes in the network.[12,15,16,19] This is achieved by taking into account *a priori* knowledge of the destination of the aircraft. More details about the merge/diverge mechanism are provided in the article.[23]

C. The PDE model

This section is based on earlier work by Bayen[18,19] et al.. We present a different numerical scheme to solve the same problem, which is more efficient than the one used in the earlier work.[18,19] Corresponding control strategies are presented in a companion article.[25] We consider aircraft density in the NAS as a continuum and study the generated flow.

We divide the airspace into line elements on which we model the density of aircraft. These line elements are called paths. We represent a path as a segment $[0, L]$ and we denote by $u(x,t)$ the number of aircraft between distances 0 and x at time t. This is sometimes referred to as "cumulated vehicle count" in the transportation literature. In particular, $u(0,t) = 0$ and $u(L,t)$ is the total number of aircraft in the path modeled by $[0, L]$ at time t. We make the additional assumption of a stationary velocity profile $v(x) > 0$ which depicts the mean velocity of aircraft flow at position x and time t. Applying the conservation of mass to a control volume comprised between positions x and $x+h$, and letting h tend to 0, one easily finds the following relation between the spatial and temporal derivatives of $u(x,t)$:

$$\begin{cases} \frac{\partial u(x,t)}{\partial t} + v(x)\frac{\partial u(x,t)}{\partial x} = q(t) & (x,t) \in (0,L) \times (0,T] \\ u(x,0) = u_0(x) & x \in [0,L] \\ u(0,t) = 0 & t \in [0,T] \end{cases}$$

where $q(t)$ represents the inflow at the entrance of the link ($x = 0$) or in terms of the density $q(t) = \rho(0,t)v(0)$, where $\rho(x,t)$ denotes aircraft density at location x and time t. This is an advection equation with control velocity and source term.

It can be shown using the method of characteristics that this partial differential equation admits a unique solution. Even though this framework is a purely continuous framework, we need to discretize it for the sake of computation.

We apply the Lax-Wendroff scheme to the preceding partial differential equation. We use a discrete grid on the domain $[0, L] \times [0, T]$:

$$x_i = \frac{iL}{M}, \quad 0 \leqslant i \leqslant M \text{ and } t_j = \frac{jT}{N}, \quad 0 \leqslant j \leqslant N$$

The Lax-Wendroff numerical scheme is based on the second order Taylor series expansion of $u(x, t)$

$$u(x, t_{j+1}) = u(x, t_j) + (\Delta t)u_t(x, t_j) + \frac{1}{2}(\Delta t)^2 u_{tt}(x, t_j) + \dots$$

Given that $u(x, t)$ is a solution of the partial differential equation above, we have:

$$u_t(x, t) = -v(x)u_x(x, t) - v'(x)u(x, t)$$

$$u_{tt}(x, t) = -v(x)u_{xt}(x, t) - v'(x)u_t(x, t)$$

If we differentiate the expression of $u_t(x, t)$ with respect to x , we obtain: $u_{xt}(x, t) = -v(x)u_{xx}(x, t) - v''(x)u(x, t) - 2v'(x)u_x(x, t)$ which yields:

$$u_{tt}(x, t) = v^2(x)u_{xx}(x, t) + 3v(x)v'(x)u_x(x, t) + (v(x)v''(x) + (v'(x))^2)u(x, t)$$

Using the preceding expressions of $u_t(x, t)$ and $u_{tt}(x, t)$ in the Taylor series expansion, we find:

$$u(x, t_{j+1}) = u(x, t_j) - (\Delta t)v(x)u_x(x, t_j) - (\Delta t)v'(x)u(x, t_j)$$

$$+\frac{1}{2}(\Delta t)^2(v^2(x)u_{xx}(x, t_j) + 3v(x)v'(x)u_x(x, t_j) + (v(x)v''(x) + (v'(x))^2)u(x, t_j)) + \dots$$

Then we replace the spatial derivatives by central finite difference approximations:

$$u_x(x, t) \leftrightarrow \frac{u^j_{i+1} - u^j_{i-1}}{2\Delta x}$$

$$u_{xx}(x, t) \leftrightarrow \frac{u^j_{i-1} - 2u^j_i + u^j_{i+1}}{(\Delta x)^2}$$

We eventually obtain the Lax-Wendroff scheme:

$$u^{j+1}_i = (1 - (\Delta t)v'(x_i) + \frac{(\Delta t)^2}{2}(v'(x_i))^2)u^j_i + \frac{\Delta t}{2\Delta x}v(x_i)(\frac{3}{2}(\Delta t)v'(x_i) - 1)(u^j_{i+1} - u^j_{i-1})$$
$$+\frac{1}{2}\left(\frac{\Delta t}{\Delta x}\right)^2 v^2(x_i)(u^j_{i-1} - 2u^j_i + u^j_{i+1})$$

The initial condition implies:

$$u^0_i = \frac{1}{2\Delta x}\int_{x_{i-1}}^{x_{i+1}} u_0(x)dx \text{ for } 0 \leqslant i \leqslant M$$

The boundary conditions are implemented using 2 ghost-cells on the left and right of the spatial domain. Given that the velocity is always positive, the boundary conditions can only be prescribed on the left; we use zero-order extrapolation for the right boundary condition:

$$u^j_{-1} = \frac{1}{\Delta t}\int_{t_j}^{t_{j+1}} \frac{q(t)}{v(0)}dt \text{ and } u^j_{M+1} = u^j_M \text{ for } 1 \leqslant j \leqslant N$$

Finally, when choosing the space and time steps, the CFL (Courant-Friedrichs-Lewy) condition has to be verified:

$$\left|\frac{v(x)\Delta t}{\Delta x}\right| \leqslant 1 \text{ for } x \in [0, L]$$

$\left|\frac{v(x)\Delta t}{\Delta x}\right|$ is called the Courant number. The Lax-Wendroff scheme will be increasingly accurate as the Courant number approaches to 1 and the time and space steps should be chosen so that:

$$\frac{\Delta t}{\Delta x} \text{ is slightly smaller than } \frac{1}{\sup_{x\in[0,L]} v(x)} \quad .$$

D. A benchmark example for comparison of the three models

For the comparison, the three models described above are implemented on the same aggregate traffic flow graph model depicted in Figure 3. The construction of the graph is outlined in the articles.[23,24] The portion of airspace of interest for this study is depicted in Figure 1, and consists of 23 sectors of the Oakland, Los Angeles, Seattle and Salt Lake City Centers. The graph identification procedure relies on the notion of *path*, illustrated in Figure 2. We use one year of ASDI/ETMS data for this identification, which results in the graph shown in Figure 3. For the MMM, we will use β splits at the nodes where traffic is diverging, following the procedure outlined in their original article[12] modified according to Section II A. For the two other models, we will use the notion of paths, linking any origin to any destination in the graph. This idea was suggested to us by Dr. George Meyer, and is sometimes referred to as the *colored flow paradigm*. This enables us to avoid the identification of the β split parameters, and the resulting inaccuracies of this model.

Using the terminology in Figure 2, the graph used for this study has 217 paths, 102 links, 4069 cells (MMM), 10293 cells (delay model), and 43400 grid points (PDE model). It consists of 10 high altitude sectors, includes three major airports (SFO, SJC and OAK). The number of flights used for this study for a single day is on the order of 8000.

The parameter identification used for the MMM is straightforward: following the work of the authors of the MMM[14] we average all velocities of all aircraft over one year for the airspace of interest. For the delay model and the PDE model, we do it path by path. An example of velocity fit for one path is shown in Figure 4. The β split coefficients used for the MMM are computed by dividing the number of aircraft on a branch from a split by the total number of aircraft exiting the split. The cell dimension in the MMM is computed as the distance traveled by an aircraft in one minute (our time step in the simulation). Since the average velocity is 380 knots, this gives the cell dimension to be 11 km. For the delay system model, the cell dimension is time-based and is one minute in length.

The inflow conditions for the three models are extracted from the ASDI/ETMS data for one day. Each flight in the data is analyzed in terms of its time of arrival in one of the sectors under consideration. Additionally, the delay system model and the PDE model also analyze a flight path according to the details in the earlier work.[23,24]

III. Model validation

The models are validated against ASDI/ETMS data and their respective performances are compared. Simulations are performed from 8:00am GMT on January 24th, 2005 to 8:00am GMT on January 25th, 2005. The input to the models is the number of aircraft entering the considered region (Oakland Center). The predicted states are computed from each model and compared with the recorded data.

Sector counts predicted by the three models are first compared with the recorded air traffic data (ASDI/ETMS). Our study shows that all the sector counts predicted by the three models and ASDI data differ by noise of a non-negligible magnitude for the following reasons: (1) for the delay system model, the travel time on a link in the network is computed as the average travel time for all flights in the data set used for the identification; (2) for the PDE model, the velocity profile of each path is filtered from sampled velocities and only several modes are preserved; (3) for the MMM, the split ratios are computed from historical data which usually do not match the instantaneous ratios for a specific day and also the MMM assumes a uniform velocity across the whole network.

A *Moving average filter* (MAF) technique is used to filter the sector counts for both the recorded ASDI/ETMS data and the models' simulation data. Applying a MAF to the data requires an appropri-

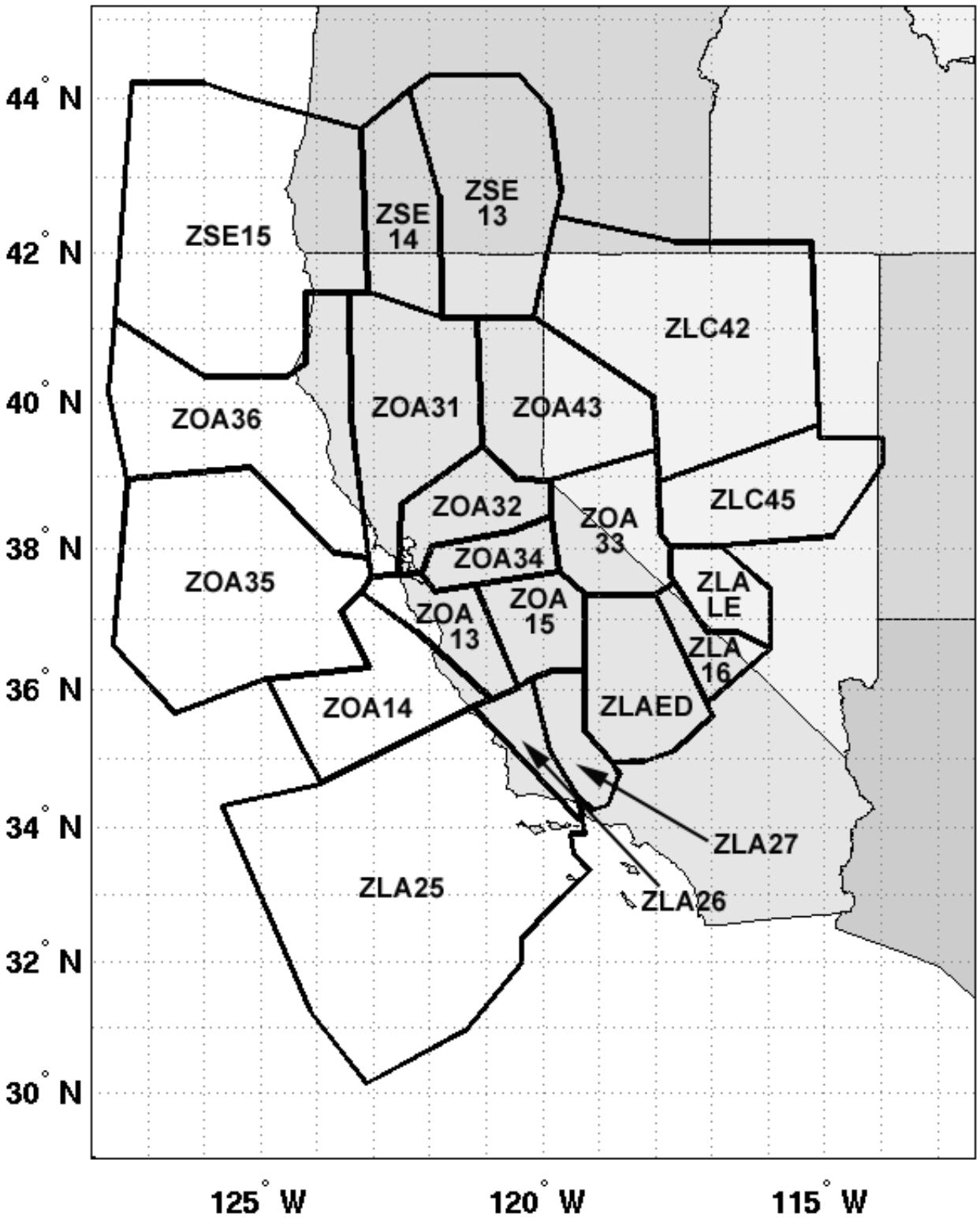

Figure 1. *Map of the region of the airspace considered in this study: the Oakland ARTCC, called ZOA, a portion of Los Angeles ARTCC, called ZLA, a portion of Salt Lake City ARTCC, called ZLC, and a portion of Seattle ARTCC, called ZSE.*

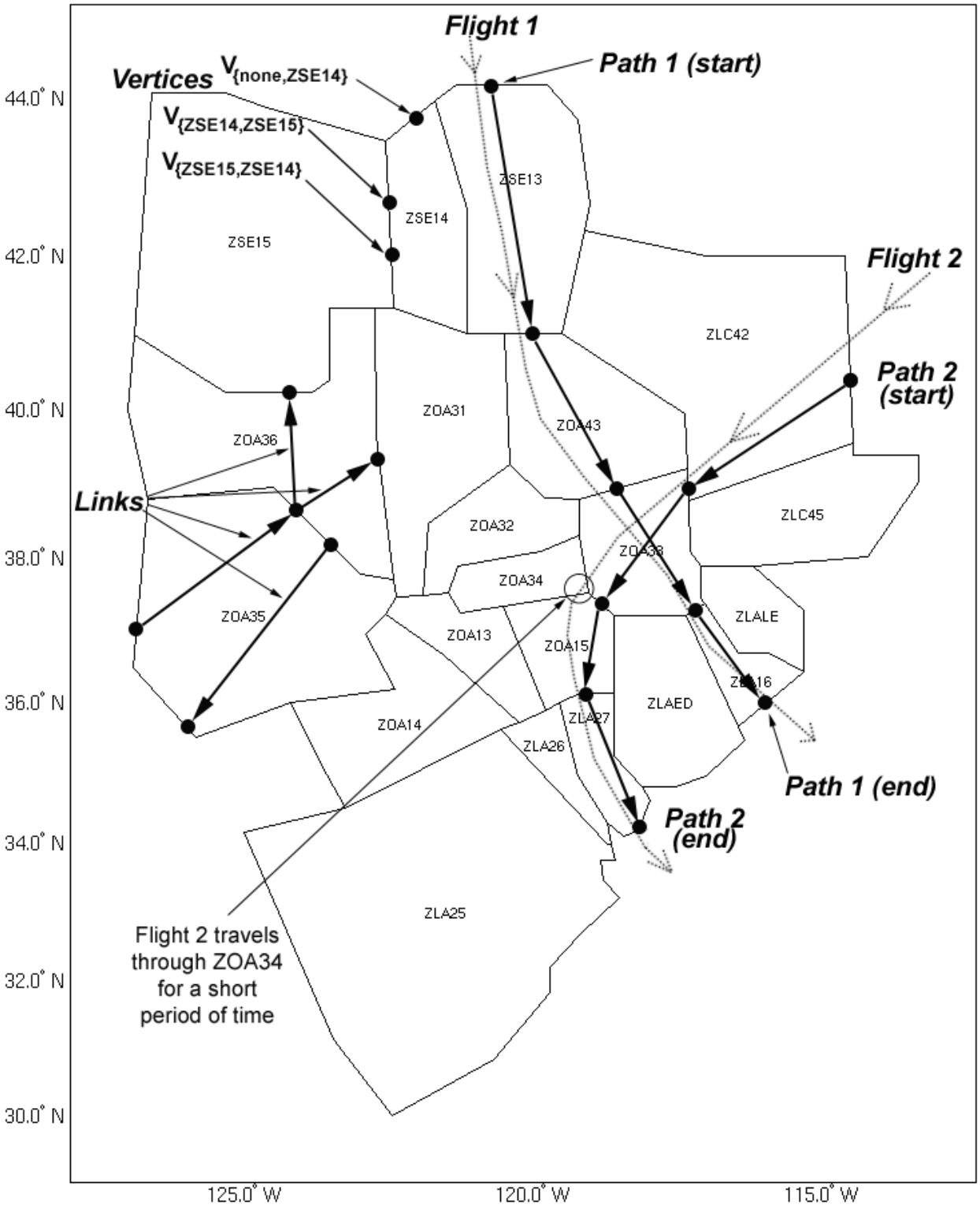

Figure 2. *Examples of vertices and links; trajectories and paths.*

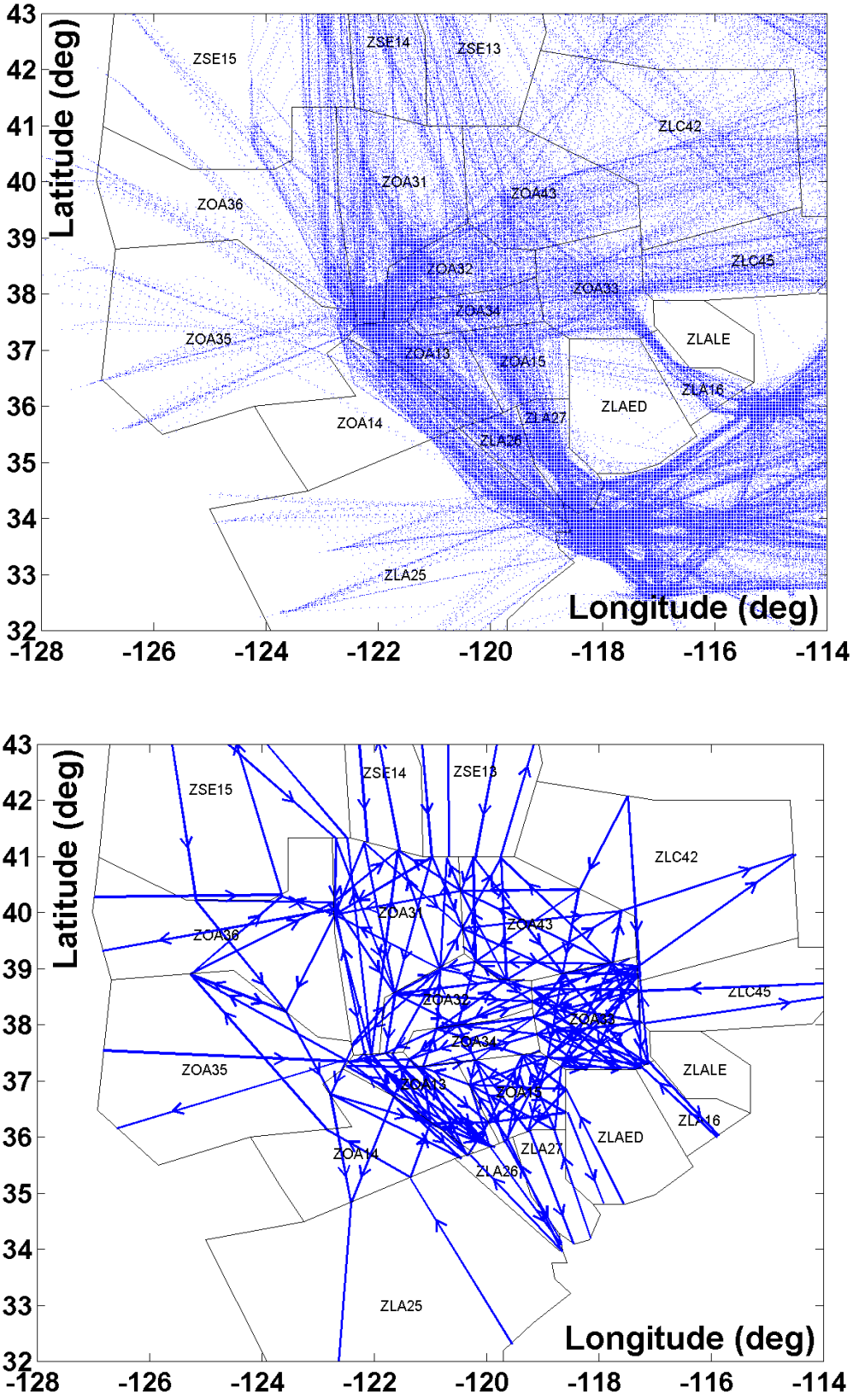

Figure 3. Top: *An example of flight tracks in Oakland Center and nearby airspace.* **Bottom:** *Graph model representing the flow patterns above, composed of 312 links.*

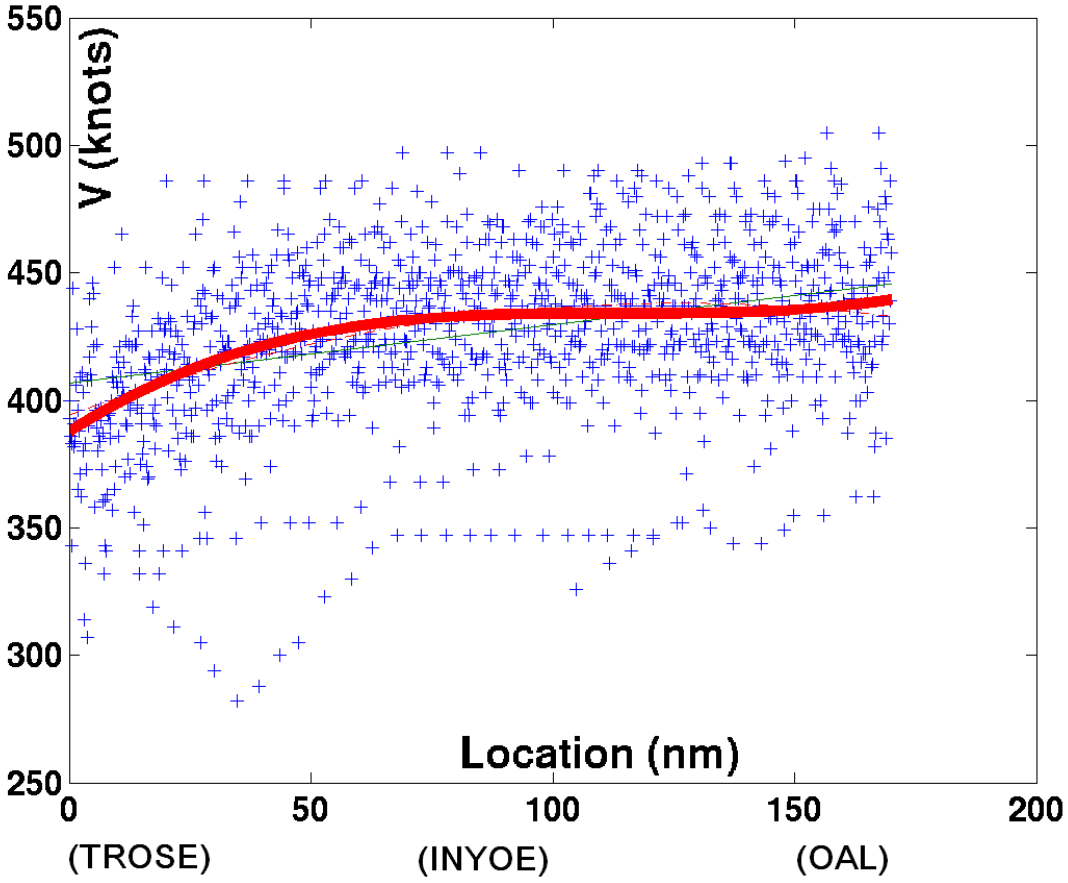

Figure 4. ***A typical velocity profile along a path.*** x**-axis***: positions from the starting point of a path in the model;* y**-axis***: velocities in knots. A third order curve is used to fit the velocity profile. Typically, flights going through this path (passing through way-points TROSE-INYOE-OAL) pop-up from low altitude airspace and climb up to high altitudes.*

ate number of data points (time window) in the average. A small time window captures the dynamics of the flow errors but loses the "filtering" benefits, while a large time window filters noise but destroys the error dynamics. To determine a proper size of time window, an experiment involving the maximum sector count error is performed. The maximum count error is the maximum error computed as the absolute difference between the model's sector count and the actual sector count computed from the recorded ASDI/ETMS data, over the course of a simulation. The model chosen to determine the time window does not make significant difference. Figure 5 shows the results obtained using the PDE model. It shows how the maximum error decreases as the time window (number of data points in the average) increases. Note that for most sectors, the maximum errors are below two when the time window is 30 minutes, and above 30 minutes, increasing time window does not help much decrease the maximum error, and does not make sense for the problem of interest as well. For this reason, 30 is chosen as the number of data points in the average (the time window, or time span). Removing noise makes physical sense for this problem. Indeed, very often, sector count exceeds legal values for a few minutes (if aircraft are about to exit a sector), which is tolerated in practice, as such flights usually do not pose significant problems to air traffic controllers.

Figure 6 shows an example of the unfiltered raw data overlayed with the filtered data using MAF. As can be seen, a significant portion of the noise in the data can be removed by performing a MAF of the data, which makes it more suitable for analysis and comparison.

Figure 7 shows the predicted and actual sector counts as a function of time in four sectors: medium loaded sectors ZOA32, ZOA34, highly loaded sector ZOA33, and low traffic sector ZOA35. The data shown in the figure is filtered by MAF. From the figures we can see that all the models correctly predict the trends

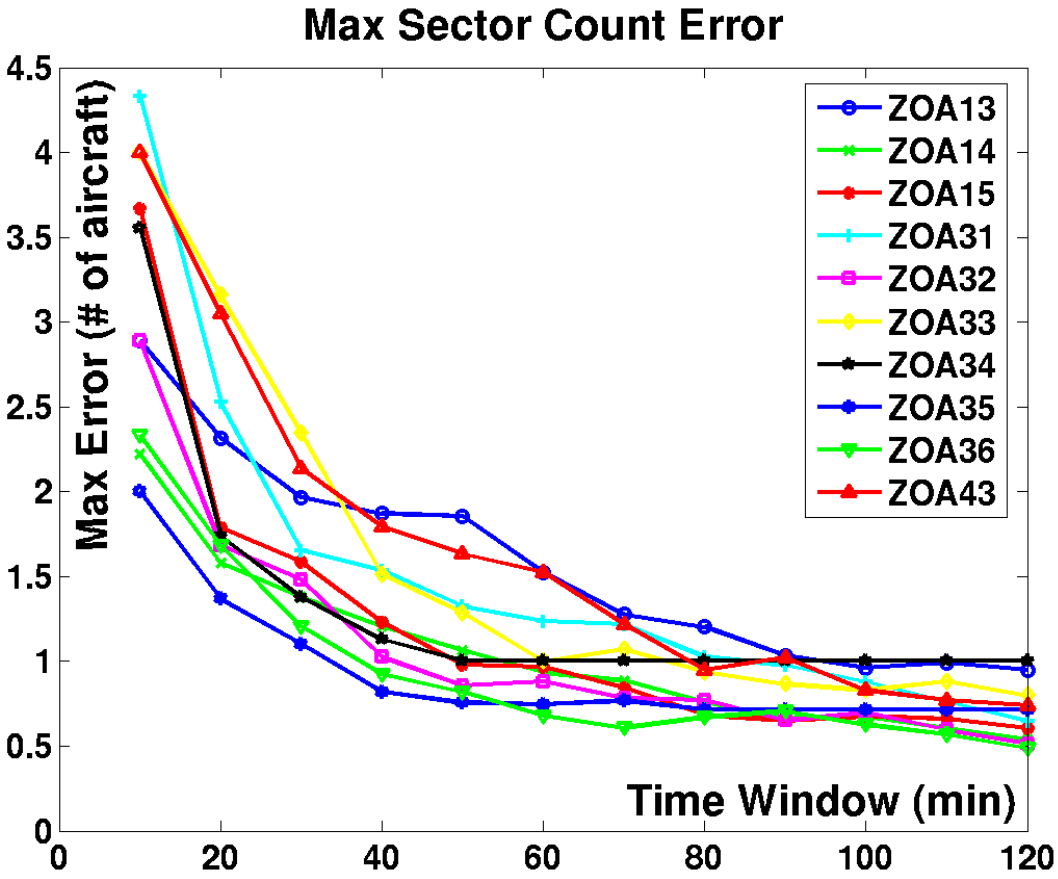

Figure 5. *Maximum sector count error between simulation of the PDE model and ASDI/ETMS data (after filtering). The maximum error decreases as the time window increases.*

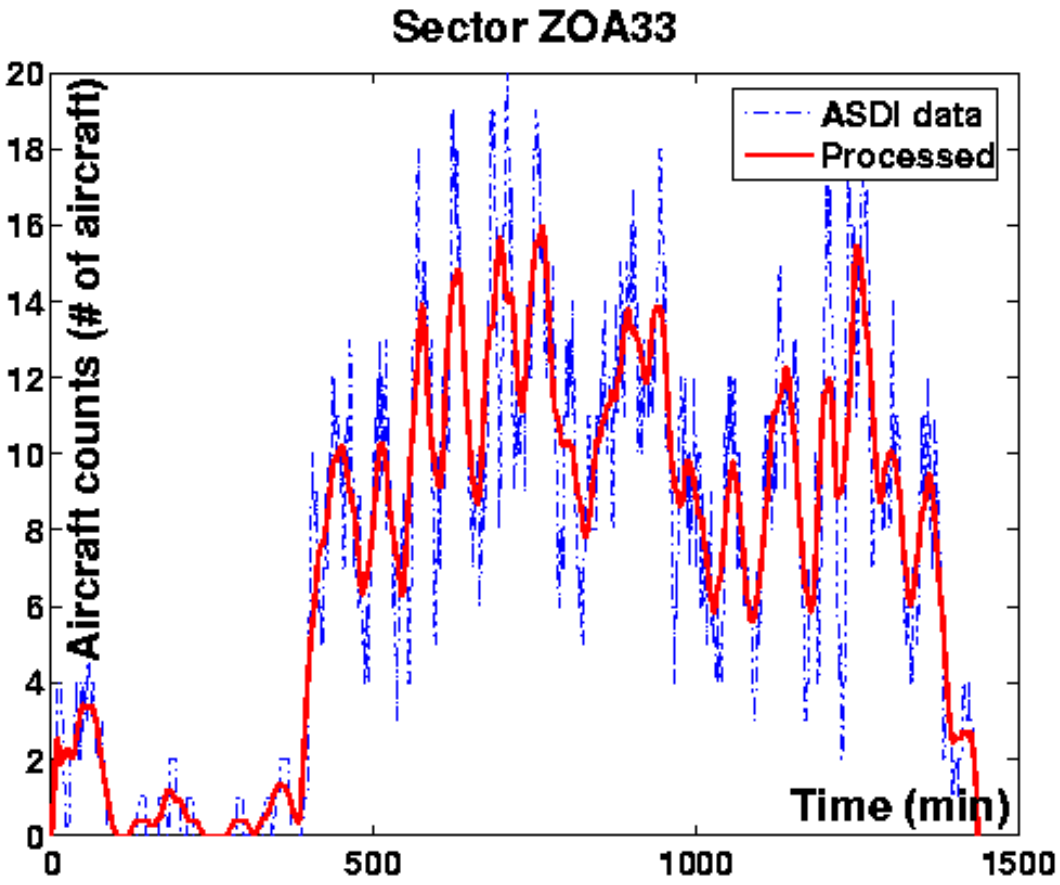

Figure 6. *Moving average filter (MAF): the dotted curve represents the unfiltered sector counts of sector ZOA33, and the solid curve represents the filtered data using a time window of 30 minutes.*

of sector counts.

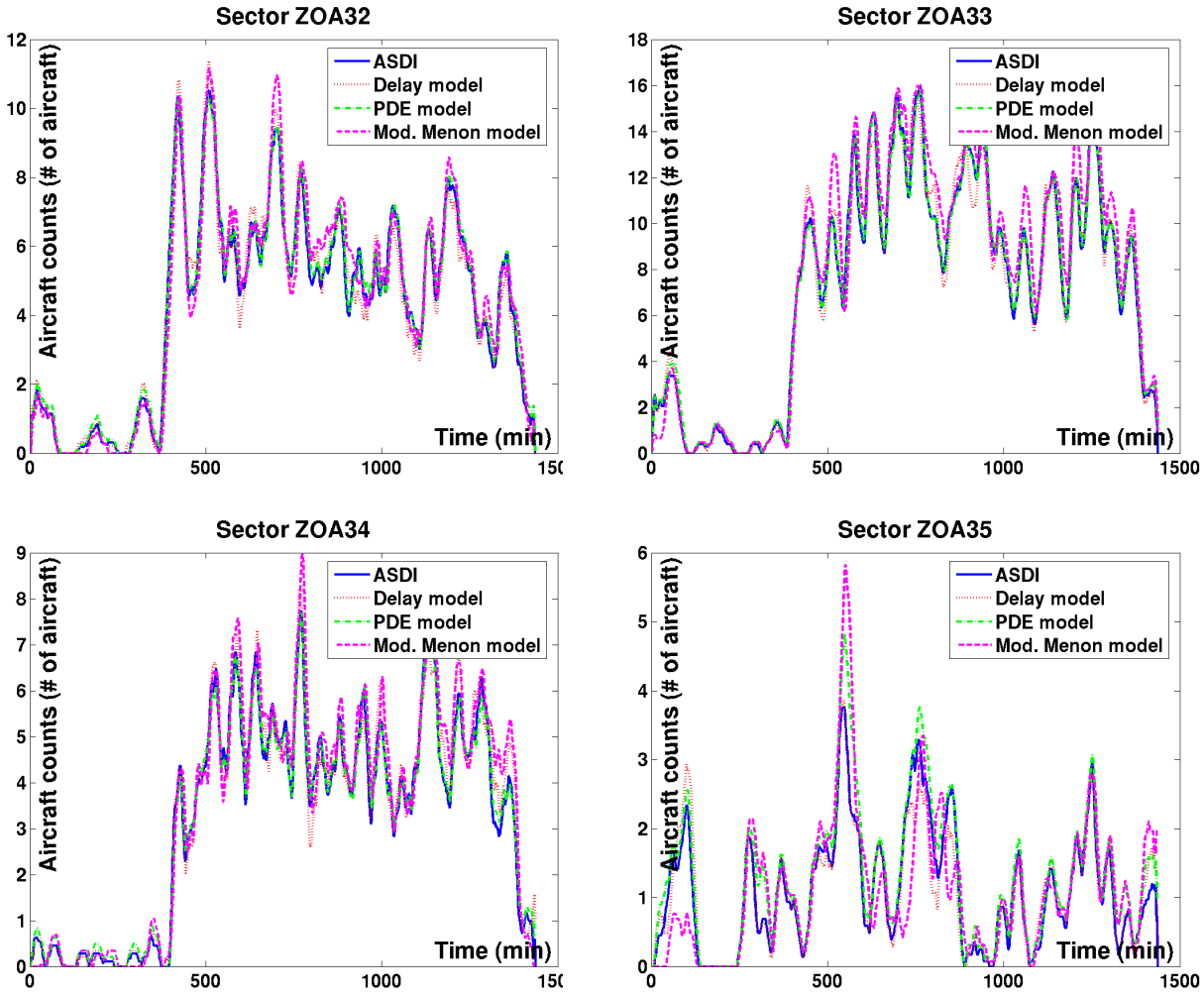

Figure 7. ***Comparison of the predictions of aircraft sector counts with the three models and the ASDI/ETMS data. Curves represent the processed sector counts after filtering.***

A similar comparison is done with inflows into the sectors. Inflows represent the number of aircraft entering a certain sector in a unit of time (one minute in our study). For example, for ZOA33, the inflows count the number of aircraft arrivals from sectors ZOA15, ZOA34, ZOA32, ZOA43, ZLC42, ZLC45, ZLALE, ZLA16, ZLAED, as well as flights originating in ZOA33 (please refer to Figure 1). Figure 8 shows the predicted inflows into four sectors (ZOA32, ZOA33, ZOA34 and ZOA35), as well as the inflows computed from the recorded ASDI/ETMS data, into these three sectors. The curve in each plot represents the filtered inflows. From the figures we can see that all the models correctly predict the trends of the inflows into sectors.

IV. Comparison

From Figures 7 and 8, we can see that the PDE model displays the best prediction capabilities among all the models. As can be seen in Figures 7 and 8, the sector count and inflow predictions of the PDE model are closer to the recorded ASDI/ETMS data, compared with the other two. In comparing the three models we will quantify each model's error as well as their computational efficiency.

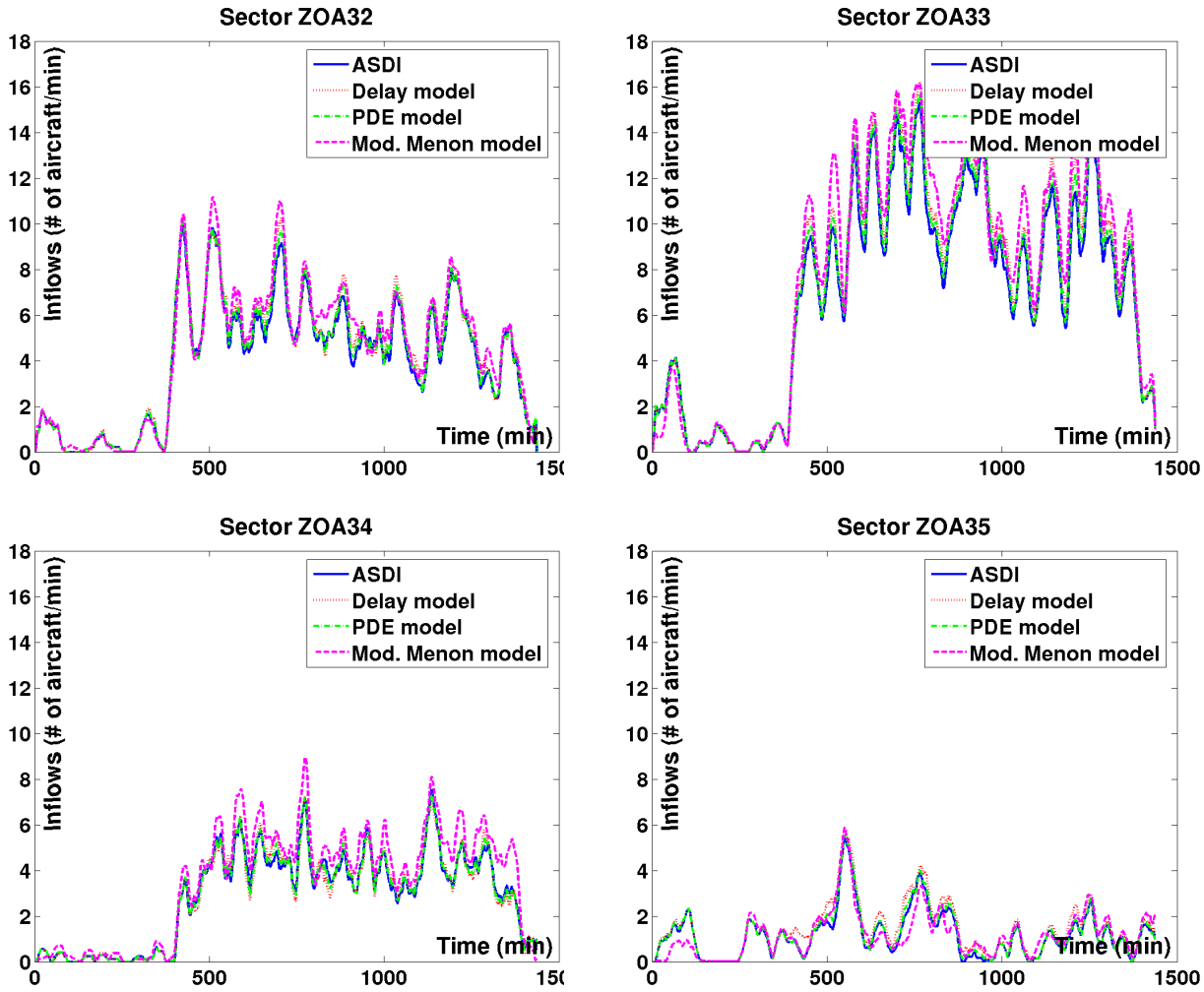

Figure 8. *Comparison of the predictions of the sector inflows with the three models and the ASDI/ETMS data. Curves represent the processed inflows after filtering.*

A. Error analysis

The error analysis involves two comparisons: cumulated occurrence of sector count error breach (S), and the instantaneous sector count error. Following the article,[24] S is defined as the summation of time intervals under the condition that difference of sector counts between the simulation and ASDI/ETMS data is greater than or equal to a user-specified capacity limitation, within a certain time window. This is summarized in equation (12):

$$S = \sum_{k=1}^{T} \mathbb{I}_{\{|y_{\text{sim}}(k) - y_{\text{ASDI/ETMS}}(k)| \geq C_s\}} \tag{12}$$

where $\mathbb{I}$ represents the indicator function. The sector count is denoted by $y(k)$, ASDI/ETMS and simulated. The constant C_s is a user-defined threshold. The time window we choose in our simulation is 1440 minutes (24 hours), i.e. $T = 1440$. To measure the similarity in the simulation and the ASDI/ETMS data, different values of C_s are used, and plots of percentage of breaches versus C_s are shown in Figure 9. For example, if we choose $C_s = 3$, the percentage of breaches of the MMM in sector ZOA32 is 15%, which means the predicted sector counts in ZOA32 by the MMM differ from the ASDI/ETMS data by at least three aircraft for 15% of the time. As the value of C_s increases, the breach length for each model tends to zero. This is because C_s is the aircraft count error limit. The PDE model is close to zero breach when the aircraft count error limit is less than five, which has the best predictive performance. The aircraft count error limits to bring the delay system model and the MMM to zero breach are higher than the PDE model. The reason for this will be explained in a later section.

The instantaneous sector count error analysis is performed as well. This error is the difference between the models' aircraft count and the actual aircraft count for each sector computed from the recorded ASDI/ETMS data at each time step in the simulation. The corresponding relative error is the ratio between the absolute instantaneous error and the actual count. The instantaneous error and relative error are shown for sectors ZOA32, ZOA33 and ZOA34 in Figure 10.

Number	1	2	3	4	5	6	7	8	9	10
Name	ZOA13	ZOA14	ZOA15	ZOA31	ZOA32	ZOA33	ZOA34	ZOA35	ZOA36	ZOA43

Table 1. ***Indices for the considered sectors in Oakland Center (numbers refer to Figure 11).***

Figure 11 shows a summary of the max/mean error of the sector counts, and the error variance as well. From Figure 11 we can see that the PDE model experiences less error and less variance than both the other two.

B. Computational efficiency

For all three models, it takes approximately ten minutes to convert the aggregate traffic flow graph model referred to in Section II D according to each model's specifications. Table 2 lists the CPU time and memory usage for the three models to predict inflows and sector counts. The analysis is done for 10 high altitude sectors in the Oakland Center, for each minute over 24 hours embedded in a set of 23 high altitude sectors, in order to eliminate undesirable boundary effects (see map in Figure 1). The computations are done on a 1.4 GHz CPU, 512 MB RAM PC running Linux, using the c++ programming language. The delay model has the fastest running time (six minutes), which is about 10 times faster than the PDE model and 15 times faster than the MMM. The difference between the delay model and the PDE model is that the time increments required for a PDE model simulation are smaller than the delay unit used in the delay model. The reason why the PDE model and the delay model are significantly faster than the MMM is that the MMM must keep track of all the merge diverge nodes in the system. In order to do this, at each time step, there are a number of matrix multiplications in that model must be computed in order to account for all merge and diverge nodes. For the PDE model and the delay model the aircraft count updates are based on only the previous counts and the path length (see Section II D).

C. Critical differences in the three models - interpretation

The previous simulations enabled the quantitative comparison of the three models presented earlier. This comparison showed several significant differences in the respective performances of the models, which we

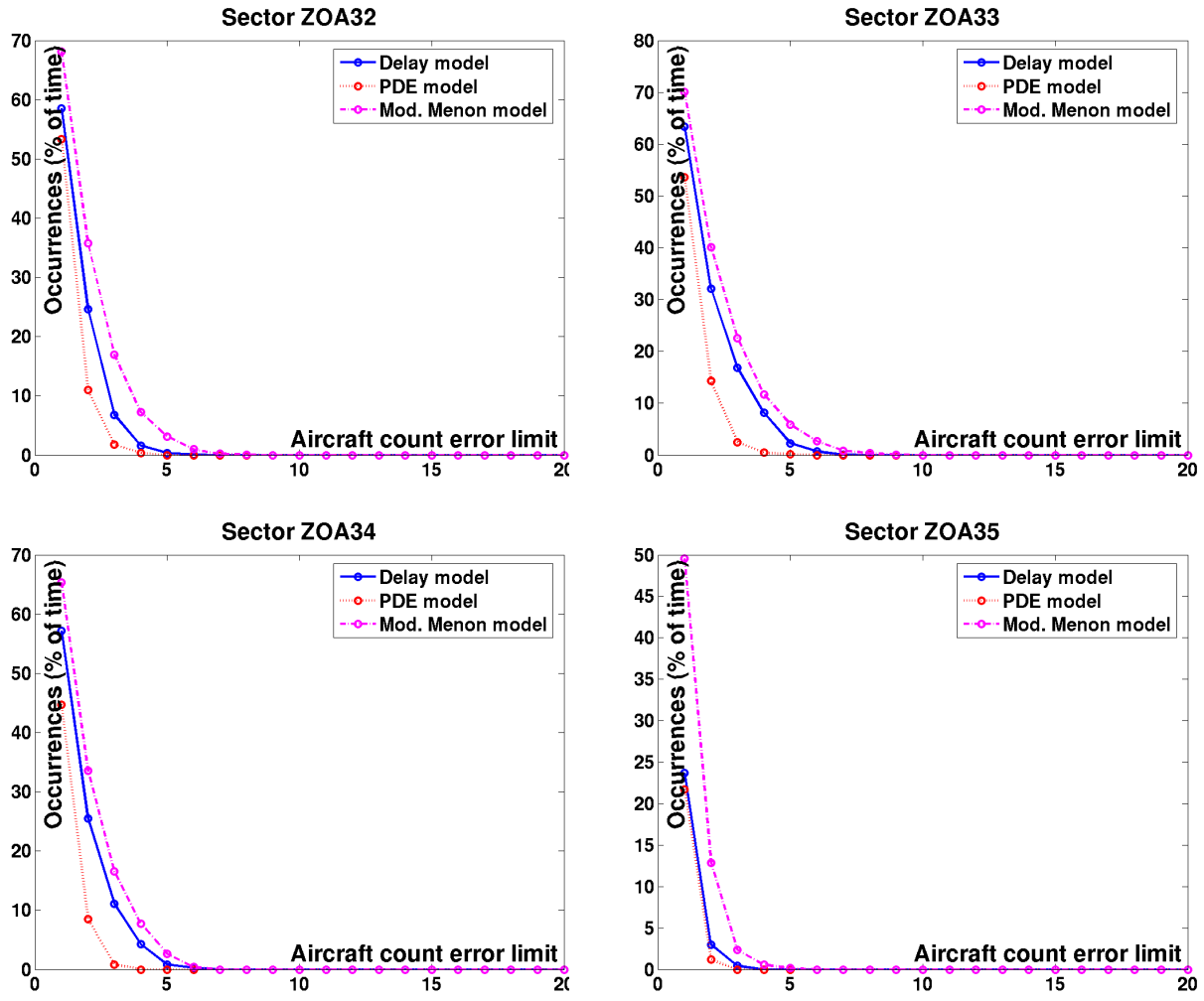

Figure 9. *Occurrences of breach of sector count error for four sectors in the Oakland Center (unit is % of the time).*

	Delay model	PDE model	MMM
CPU time (minutes)	6	50	90
Max memory usage (MegaBytes)	395	481	376

Table 2. ***Computational efficiency (runs performed on a 1.4 GHz CPU, 512 MB RAM PC running Linux, using c++).***

now summarize and explain:

1. One evident result stands out: the PDE model consistently outperforms both of the other two models and the delay system model is the second. The PDE model incorporates the continuous dynamics of aircraft, which is close to the physics of the flows and considers aircraft density in the NAS as a continuum and studies the generated flows, which explains its higher order of accuracy. Even if it performs better in terms of accuracy, the underlying mathematical framework used (PDEs) forces us to use sophisticated optimization techniques to perform optimal TFM policy synthesis. This is illustrated in a companion article.[25] There is thus obviously a tradeoff between accuracy and efficiency.

2. In terms of the velocity of aircraft flow, the modified Menon model is less accurate while the PDE model is the finest. The modified Menon model uses an average velocity as the speed of all aircraft in the model, which is a first order approximation. The delay system model assumes average velocities on a given *link*. So, a particular path, composed of consecutive links, has different speeds, corresponding to successive portions of the flight (climb, cruise, descent). Therefore the delay system model has more flexibility than the modified Menon model in describing features of the flows. For the PDE model, the velocity along a link is computed using least-squares and is continuous along a path (see Section II D for more details).

3. In terms of the diverge nodes, the modified Menon model is also the roughest while the PDE model and delay system model are finer. The modified Menon model computes a fixed ratio of outgoing flow at a diverge node based on the data set. This is a fundamental issue of Eulerian models, which was resolved using the *colored flow diagram* of Dr. George Meyer. The PDE model and the delay system model generate a path through the network for each incoming flight, as outlined in article.[24]

V. Conclusion

Three Eulerian models are implemented on a network graph model of air traffic flow. Adaptations are made to the models to fit the general network topology. The models are applied to high altitude traffic for a full Air Traffic Control Center of the National Airspace System. Each model is implemented on the same aggregate traffic flow graph model and simulated over an entire day. Compared to flight data, the models show good predictive capabilities. The models are also compared to each other in terms of their predictive ability, computation time and memory requirements.

Future work will include implementation of Menon 2D model[26] and will be to use a full year of ASDI/ETMS data to study hourly/weekly patterns of air traffic flows to show how using these patterns can improve the respective predictive capabilities of each of the models. More simulations, including different days and controlled experiments, will be run in order to underline the strengths and weaknesses of each model. The network graph model will be extended to incorporate NAS-wide studies. We will also add *Ground Delay Programs* (GDP) and airports, such as airport capacities and constraints in the formulation of the model.

Acknowledgments

This work was supported by NASA under Task Order TO.048.0.BS.AF. We are thankful to Dr. Shon Grabbe for his help with ASDI/ETMS data and FACET. We are grateful to Dr. Gano Chatterji for his suggestions regarding the models of the National Airspace System. We want to acknowledge Dr. George Meyer for fruitful conversations on air traffic control and his ongoing support for our research, and to Charles-Antoine Robelin for his help with generating the initial model, sharing his source code and helping with the graphs presented in this article. We are thankful to Dave Knorr (FAA) for providing us a full year of ASDI data and to Doug Williamson (CNA) for his technical support with the data. We are grateful to Larry Hogle and Bill Berry for helping with the collaboration between UC Berkeley and NASA Ames through the UARC.

References

[1]Nolan, M. S., *Fundamentals of Air Traffic Control*, Brooks Cole, 4th ed.

[2]Devasia, S., Heymann, M., and Meyer, G., "Automation Procedures for Air Traffic Management: A Token-Based Approach," *Proceedings of the American Control Conference*, Anchorage, AK, May 2002, pp. 736–741.

[3]Bayen, A., Grieder, P., Meyer, G., and Tomlin, C. J., "Langrangian Delay Predictive Model for Sector-Based Air Traffic Flow," *AIAA Journal of Guidance, Control and Dynamics*, Vol. 28, No. 5, 2005, pp. 1015–1026.

[4]Menon, P. K., Sweriduk, G. D., and Bilimoria, K., "A new approach for modeling, analysis and control of air traffic flow," *AIAA Conference on Guidance, Navigation, and Control*, Monterey, CA, August 2002, AIAA Paper 2002–5012.

[5]Lighthill, M. J. and Whitham, G. B., "On kinematic waves. II. A Theory of traffic flow on long crowded roads," *Proceedings of the Royal Society of London*, Vol. 229, No. 1178, 1956, pp. 317–345.

[6]Richards, P. I., "Shock waves on the highway," *Operations Research*, Vol. 4, No. 1, 1956, pp. 42–51.

[7]Daganzo, C., "The cell transmission model: a dynamic representation of highway traffic consistent with the hydrodynamic theory," *Transportation Research*, Vol. 28B, No. 4, 1994, pp. 269–287.

[8]Daganzo, C., "The cell transmission model, part II: network traffic," *Transportation Research*, Vol. 29B, No. 2, 1995, pp. 79–93.

[9]Strub, I. and Bayen, A., "Mixed Initial-Boundary Value Problems for Scalar Conservation Laws: Application to the Modeling of Transportation Networks," *Hybrid Systems: Computation and Control*, edited by J. Hespanha and A. Tiwari, No. 3927 in Lecture Notes in Computer Sciences, Springer Verlag, March 2006.

[10]Menon, P. K., Sweriduk, G. D., Lam, T., and Cheng, V. H. L., "Air traffic flow modeling, analysis and control," *AIAA Conference on Guidance, Navigation, and Control Conference and Exhibit*, Austin, TX, August 2003, AIAA Paper 2003–5712.

[11]Menon, P. K., Sweriduk, G. D., Lam, T., Diaz, G. M., and Bilimoria, K. D., "Computer-aided Eulerian air traffic flow modeling and predictive control," *AIAA Conference on Guidance, Navigation, and Control*, Providence, RI, August 2004, AIAA Paper 2004–2683.

[12]Menon, P. K., Sweriduk, G. D., and Bilimoria, K., "New approach for modeling, analysis and control of air traffic flow," *AIAA Journal of Guidance, Control and Dynamics*, Vol. 27, No. 5, 2004, pp. 737–744.

[13]Sridhar, B. and Menon, P. K., "Comparison of linear dynamic models for air traffic flow management," 16^{th} *IFAC world congress*, Prague, Czech, July 2005.

[14]Menon, P. K., Sweriduk, G. D., and Bilimoria, K., "New approach for modeling, analysis and control of air traffic flow," *AIAA Journal of Guidance, Control and Dynamics*, Vol. 27, No. 5, 2004, pp. 737–744.

[15]Roy, S., Sridhar, B., and Verghese, G. C., "An Aggregate Dynamic Stochastic Model for Air Traffic Control," *Proceedings of the* 5^{th} *USA/Europe ATM 2003 R&D Seminar*, Budapest, Hungary, June 2003.

[16]Sridhar, B., Soni, T., Sheth, K., and Chatterji, G., "Aggregate Flow Model for Air-Traffic Management," *AIAA Journal of Guidance, Control and Dynamics*, Vol. 29, No. 4, 2006, pp. 992–997.

[17]Robelin, C., Sun, D., Wu, G., and Bayen, A. M., "En-Route Air Traffic Modeling and Strategic Flow Management using Mixed Integer Linear Programming," *INFORMS Annual Meeting 2005*, New Orleans / San Francisco, Nov. 2006.

[18]Bayen, A. M., Raffard, R. L., and Tomlin, C. J., "Adjoint-based constrained control of Eulerian transportation networks: application to Air Traffic Control," *Proceedings of the American Control Conference*, Boston, June 2004, pp. 5539–5545.

[19]Bayen, A. M., Raffard, R. L., and Tomlin, C. J., "Eulerian network model of air traffic flow in congested areas," *Proceedings of the American Control Conference*, Boston, June 2004, pp. 5520–5526.

[20]Raffard, R., Waslander, S. L., Bayen, A. M., and Tomlin, C. J., "A Cooperative, Distributed Approach to Multi-Agent Eulerian Network Control: Application to Air Traffic Management," *Proceedings of the AIAA Guidance, Navigation and Control Conference and Exhibit*, San Francisco, CA, Aug 2005, AIAA Paper 2005-6050.

[21]Raffard, R., Waslander, S. L., Bayen, A. M., and Tomlin, C. J., "Toward Efficient and Equitable Distributed Air Traffic Flow Control," *Proceedings of the American Control Conference*, Minneapolis, June 2006.

[22]Iamratanakul, D., Meyer, G., Chatterji, G., and Devasia, S., "Quantification of Airspace Sector Capacity using Decentralized Conflict," *Proceedings of the* 43^{rd} *IEEE Conference on Decision and Control*, Atlantis, Paradise Island, Bahamas, December 2004, pp. 2003–2009.

[23]Robelin, C. A., Sun, D., Wu, G., and Bayen, A. M., "Strategic Traffic Flow Models based on Data-Mining and System-Identification Techniques," NASA Technical Memorandum, in preparation, 2006.

[24]Robelin, C., Sun, D., Wu, G., and Bayen, A. M., "MILP control of aggregate Eulerian network airspace models," *Proceedings of the American Control Conference*, Minneapolis, June 2006.

[25]Strub, I. and Bayen, A., "Analysis, Simulation and Control of Air Traffic Networks Using Continuous Flow Models," *AIAA Conference on Guidance, Navigation, and Control Conference and Exhibit*, Keystone, CO, August 2006, AIAA Paper 2006-6228.

[26]Menon, P. K., Sweriduk, G. D., Lam, T., Diaz, G. M., and Bilimoria, K., "Computer-Aided Eulerian Air Traffic Flow Modeling and Predictive Control," *AIAA Journal of Guidance, Control and Dynamics*, Vol. 29, No. 1, 2006, pp. 12–19.

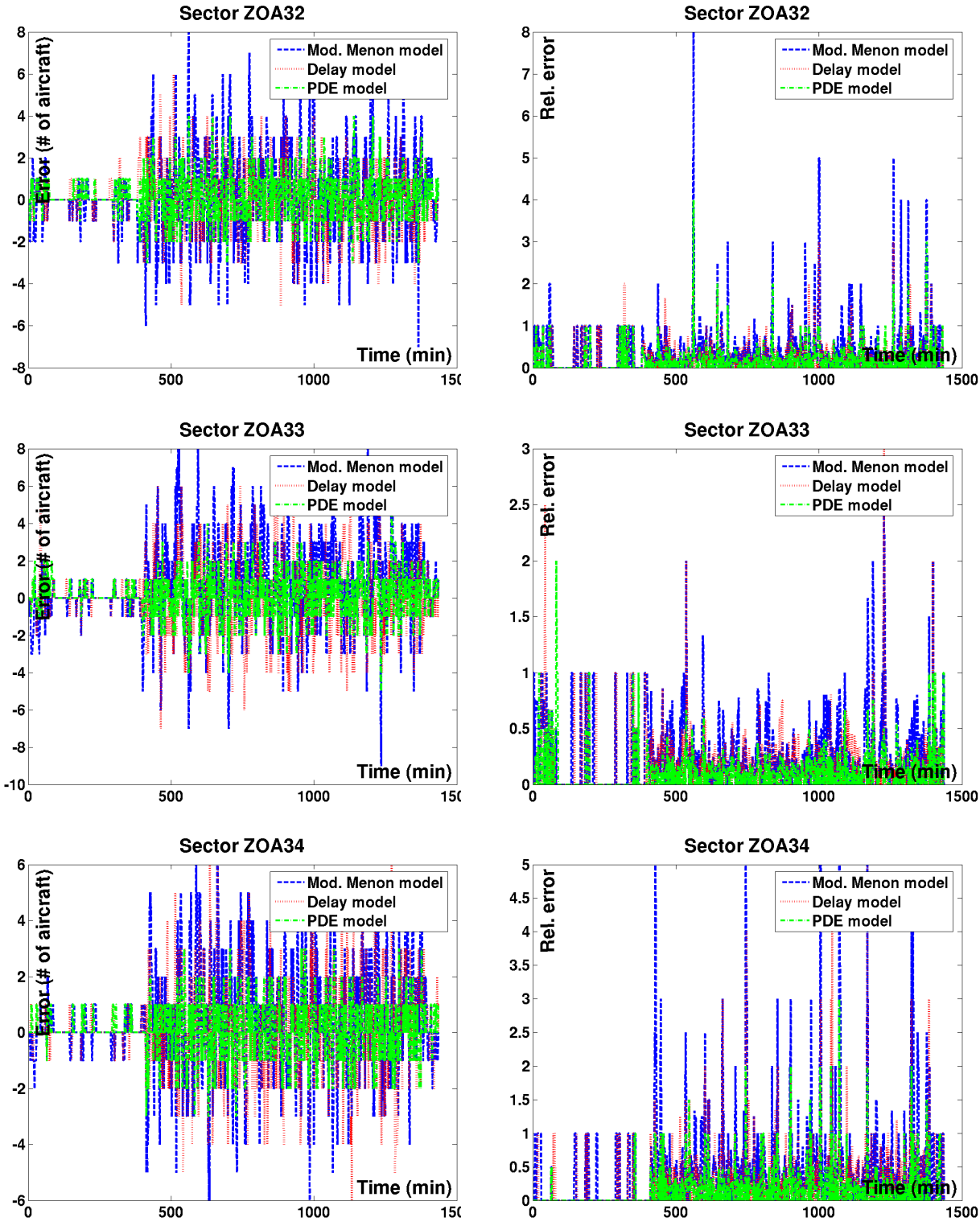

Figure 10. **Left:** *Instantaneous error for three high altitude sectors (ZOA32, ZOA33 and ZOA34).* **Right:** *Relative error for the three sectors.*

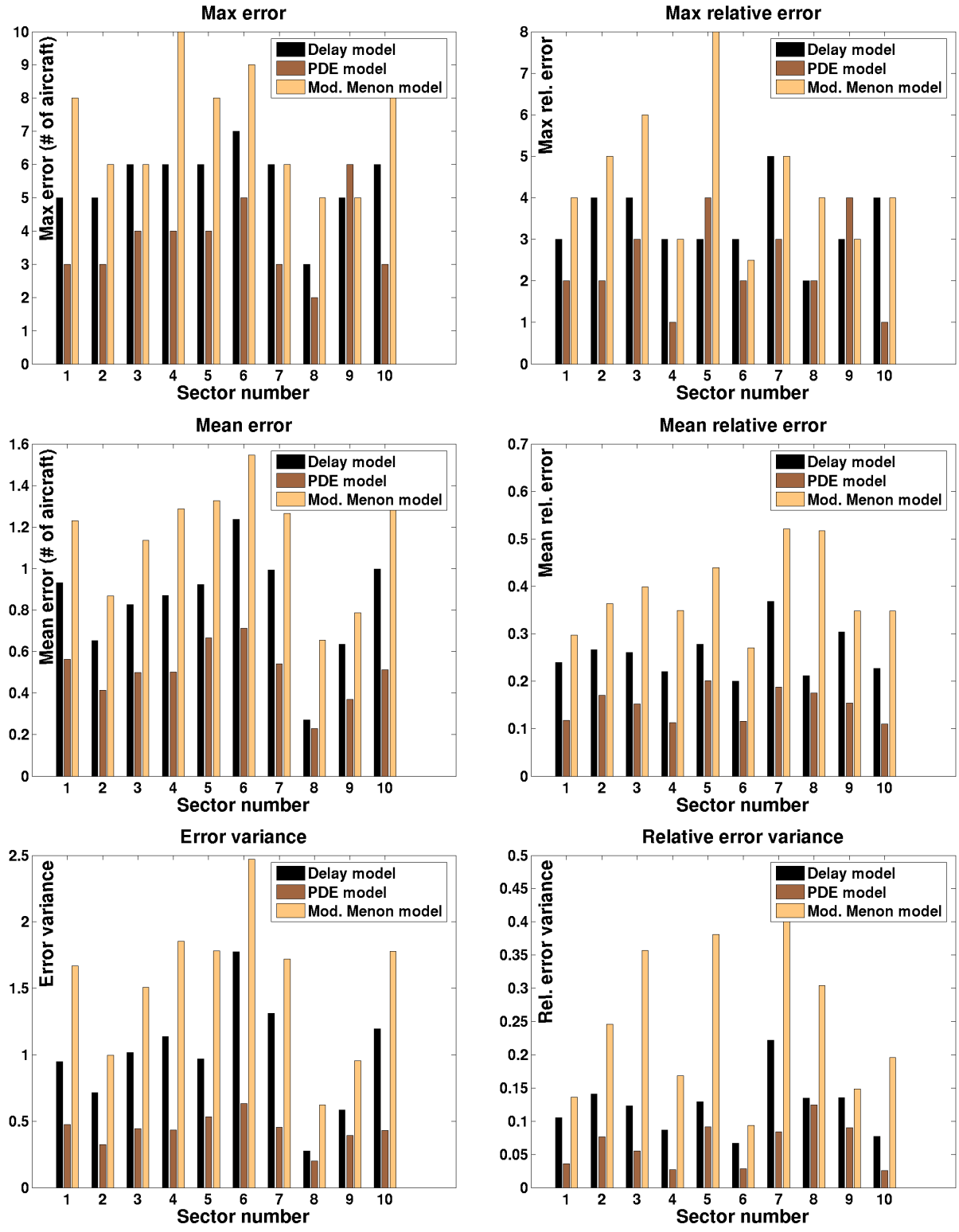

Figure 11. Left: *A summary of the absolute instantaneous error of aircraft sector count.* **Right:** *The relative error summary. Numbers on the y-axis correspond to the sectors listed in Table 1.*